Electronic Materials Letters (2020) 16:506–511
https://doi.org/10.1007/s13391-020-00238-9

ORIGINAL ARTICLE - THEORY, CHARACTERIZATION AND MODELING

Effects of Sulfur Doping on Generalized Stacking Fault Energy of Indium Phosphide

Chengru Wang[1] · Han Wu[2] · Hong Zhu[1] · Chaoying Xie[1]

Received: 9 June 2020 / Accepted: 22 July 2020 / Published online: 1 August 2020
© The Korean Institute of Metals and Materials 2020

Abstract

Indium phosphide (InP) is one of the most important optoelectronic materials, while stacking faults (SFs), as planar defects, are usually inevitable during the growth of InP possibly due to the low SF energy. As n-type dopants, sulfur atoms are generally used to change the electron concentration of InP-based devices, whereas the effects of sulfur doping on SFs of InP have not been studied in detail. In this work, the generalized stacking fault (GSF) energies of pure and sulfur-doped InP have been investigated by gliding the layers successively in the framework of first principle calculations. The results reveal the stable SF energies of InP are low and extrinsic stacking fault could be seen as the twin embryos in pure InP. Sulfur doping could decrease the GSF energies dramatically due to the lower charge density along In-S bonds than along In-P bonds, which consequently enhances the ability of twinning locally. The preferential segregation of sulfur atoms on SFs or twin boundaries could further promote the thickening of microtwin in InP. These results are of great significance to the understanding of the formation of planar defects in n-type doped III–V compounds.

Graphic Abstract

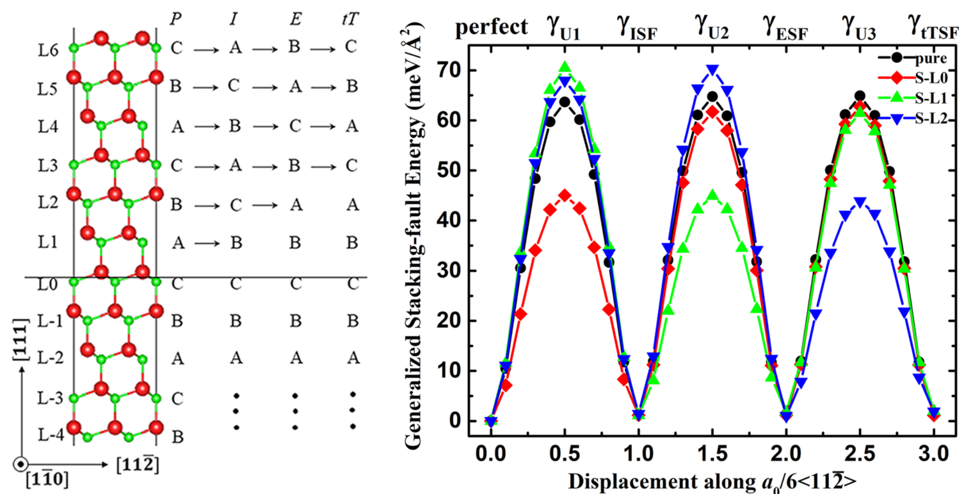

Keywords Stacking fault · Twinning ability · Sulfur doping · Segregation · Indium phosphide

✉ Hong Zhu
hong.zhu@sjtu.edu.cn

✉ Chaoying Xie
cyxie@sjtu.edu.cn

[1] School of Materials Science and Engineering, Shanghai Jiao Tong University, Shanghai 200240, China

[2] School of Physical Science and Technology, ShanghaiTech University, Shanghai 201210, China

1 Introduction

III–V semiconductors, due to the impressive optoelectronic properties, have enormous potential in electronic, optoelectronic, and photonic field [1–3]. As one of the III–V materials, high-quality indium phosphide (InP) is crucial for realizing high conversion efficiency solar cells used in space [4] and remote optical communication [3]. This benefits from the natures of the outstanding radiation tolerance [4, 5] and the lattice match between InP and III–V compounds with bandgap corresponding to the long wavelength [6]. However, stacking faults (SFs) or twin boundaries are commonly unavoidable and have a very high density in InP [7, 8]. These planar defects can configure staggering alignments of energy band [9, 10], then affecting the optoelectronic properties significantly by recombining carriers [10], trapping carriers [11, 12], or scattering electrons [13]. Nevertheless, the long-range ordered or periodic SFs are meaningful for the application of optoelectronics, which could allow to control the electrical and optical properties through introducing minibands [14].

Generally, the massive random SFs in InP could be ascribed to the low SF energy [15]. Impurities present on the interface could also give rise to the formation of SFs or microtwins in epitaxial III–V layers [16]. In addition, impurity doping is normally necessary for semiconductors to change the carrier concentration, and controllable formation of twinning superlattices could be achieved by impurity doping [17]. As n-type impurity, sulfur (S) dopants will introduce numerous microtwins, except intrinsic and extrinsic SFs, in InP crystal [18]. Many studies based on metals have shown that the formation of SFs or microtwins is depended strongly on the barrier, defined as unstable SF energy, during the glide of dislocations [19, 20], though the stable SF energies of III–V compounds have been estimated [15, 21]. Thus the generalized stacking fault (GSF) energy [22], reflecting the energy change corresponding to gliding displacement, is important to III–V compounds, just like to metals. Unfortunately, GSF energy of InP, especially S-doped InP, is still scarce, and cannot be measured directly from experiments.

In this study, the first principles calculations were performed to investigate the GSF energies of pure and S-doped InP. To our knowledge, for the first time, the size of twin embryos for pure InP was confirmed based on the convergence behavior of the GSF energy curves. In addition, the effects of S atom on the SF energies were investigated respectively for intrinsic stacking fault (ISF), extrinsic stacking fault (ESF), three-diatomic thick microtwin (tTSF) and separate twin boundary (TB). Our calculations showed that the SF energy of InP on S-doped gliding plane is reduced considerably, because of the lower charge density along In-S bonds than along In-P bonds.

2 Computational Details

As seen in Fig. 1, the InP slab supercell was established containing 44 atoms with 2 atoms per (111) atomic layer. The basis vectors X, Y and Z were set along $\left[1\ \bar{1}\ 0\right]$, $\left[11\ \bar{2}\right]$ and [111] directions respectively, in which X = $\sqrt{2}a_0/2$, Y = $\sqrt{6}a_0/2$, Z = $41\sqrt{3}a_0/12$ and a_0 is the lattice constant of InP. Then a vacuum region of 15 Å was added along the Z direction to eliminate the interaction between neighboring slabs under the periodic boundary condition. P atomic layers are denoted sequentially along [111] direction as …, L−1, L0, L1, … for elucidating the faulting/twinning pathway clearly. The SFs can only be nucleated stably on the narrowly spaced {111} planes, i.e., the gliding planes, which is indicated by the horizontal lines in Fig. 1. When the part above L0 shifts $a_0/6\left[11\ \bar{2}\right]$ distance relative to the remaining part, the original In-P bilayer stacking sequence of ABC will be destroyed and an ISF will be generated. Then repeating this process on adjacent glide plane, L1, will form an ESF. The microtwin, i.e., tTSF, can form when continue above gliding process on L2 plane. The GSF energies from perfect crystal to tTSF have been calculated based on the formula of $\gamma(b) = [E(b) - E_0]/A$ [23], where $\gamma(b)$ is the GSF energy, E_0 is the energy of perfect crystal, $E(b)$ is the energy of optimized structure, A is the shifting area, and b is the relative shifting displacement with a step of $0.1 \times a_0/6\left[11\ \bar{2}\right]$. For each displacement, the top one and bottom one layers of atoms were fixed to avoid the effects of surface relaxation, while the remaining atoms were fixed along Y direction and allowed to relax fully along X and Z directions. After testing, the 11 In-P diatomic layers (Z = $41\sqrt{3}a_0/12$) are

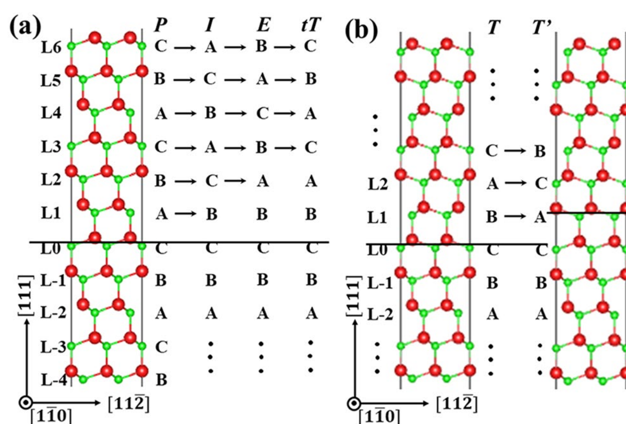

Fig. 1 The $\left[1\ \bar{1}\ 0\right]$ lateral view of InP slab models and successive shifting pathway **a** from perfect crystal (P) to tTSF (tT) and **b** on separate TB. The vacuum regions have not been displayed entirely. The large (red) and small (green) spheres indicate In and P atoms, respectively

enough thick to counteract the effect of fixing the atoms of top one and bottom one layers on the GSF energies. Additionally, the GSF energy associated with shifting on the separate TB has been calculated, as seen the schematic in Fig. 1b. In the case of doping, one P atom in the slab model with the same size of supercell as above is substituted by one S atom to study the effects of S doping on the GSF energy of InP, where the concentration of S atom is ~2.27 at%.

All the calculations were implemented with the Vienna ab-initio simulation package [24], by the method of projector augmented wave [25] combined with Perdew–Burke–Ernzerh of exchange correlation functional of generalized gradient approximation [26]. The Γ-centered k-points of $8\times4\times1$ with 500 eV energy cutoff were performed, while the convergent criteria of electronic self-consistent and ionic relaxation calculations were set to 10^{-5} eV and 0.02 eV/Å, respectively. The 4*d* states of In were treated as valence states to describe electronic distribution more precise. The lattice constant a_0 of InP was calculated to be 5.962 Å, in consistence with the reported values [27, 28].

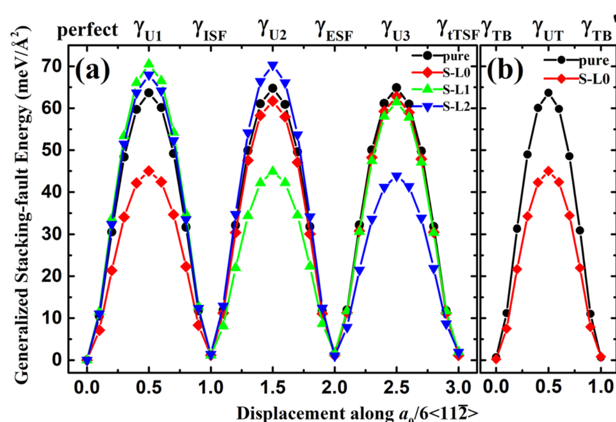

Fig. 2 **a** The GSF energy of pure and S-doped InP. The locations of S doping are at L0, L1, and L2 layer, respectively. **b** The GSF energy of the separate TB

3 Result and Discussion

3.1 The GSF Energies

Figure 2 displays the GSF energies of pure and S-doped InP. The local minimum energies along the pathway of GSF energy are defined as stable SF energies, denoted as γ_{ISF}, γ_{ESF}, γ_{tTSF} and γ_{TB} (γ_{TB}'), while unstable SF energies, denoted as γ_{U1}, γ_{U2}, γ_{U3} and γ_{UT}, indicate the energy barrier during shifting along $[11\bar{2}]$. The stable and unstable SF energies could be found in Table 1. For pure InP, the stable SF energy (γ_{ISF}) is lower than other representative III–V compounds [15]. Here, the calculated $\gamma_{ISF}=1.371$ meV/Å^2 and $\gamma_{U1}=63.665$ meV/Å^2, are comparable with the reported values [15, 28]. Two relationships of $\gamma_{ISF}\approx\gamma_{ESF}\approx\gamma_{tTSF}\approx2\gamma_{TB}$ and $\gamma_{U1}\approx\gamma_{U2}$ (γ_{U3}) $-$ $\gamma_{ISF}\approx\gamma_{UT}$ could be concluded, which implies that the interaction between two TBs (or SFs) is weak even if the separation is only one/two-diatomic layer. So, ISF and ESF could be considered as one-diatomic and two-diatomic thick microtwins, respectively. The two-diatomic thick microtwin (ESF) could be seen as twin embryo because the GSF energy begins to converge from second layer shifting ($\gamma_{tTSF}\approx\gamma_{ESF}$, $\gamma_{U3}\approx\gamma_{U2}$) [29, 30]. This suggests that energy change during subsequent thickening/shifting (three-diatomic, four-diatomic, five-diatomic, …, thick microtwin) process is similar to the transition from ISF to ESF.

In the S-doped InP, the SF energies decrease dramatically on the S-doped gliding planes, as seen in Fig. 2 and the italics in Table 1. For example, when S atom locates in L0 (S-L0), γ_{ISF} and γ_{U1} are reduced by ~14.8% and ~29.3%, respectively. This is in agreement with the scenarios of other n-type silicon [31, 32]. The relatively low unstable SF energies indicate that the gliding of partial dislocation is easier in S-doped InP than in pure InP. That is, SFs could generate in S-doped InP easily. In Table 1, the minimum values of γ_{ISF}, γ_{ESF}, γ_{tTSF}, are respectively corresponding to S-L1, S-L2 and S-L3, while these stable SF energies also have a reduction for S-L0. Conversely, the stable SF energies are nearly unchanged or even increased for other S-doped locations.

Table 1 The stable and unstable SF energies of pure and S-doped InP (units in meV/Å^2)

	γ_{U1}	γ_{ISF}	γ_{U2}	γ_{ESF}	γ_{U3}	γ_{tTSF}	λ_1	λ_2	Λ_1	Λ_2
p-InP	63.665	1.371	64.754	1.344	64.870	1.339	0.022	0.983	0.021	0.998
S-L0	*45.014*	*1.168*	61.690	*1.160*	62.769	*1.136*	0.026	0.730	0.019	0.983
S-L1	70.496	*1.156*	*44.886*	1.760	61.443	1.967	*0.016*	*1.571*	0.039	0.731
S-L2	67.969	1.407	70.342	*1.004*	*43.869*	1.914	0.021	0.966	*0.014*	*1.603*
S-L3	67.189	1.373	68.150	1.382	69.665	*0.901*	0.020	0.986	0.020	0.978
TB	p-InP	$\gamma_{TB}=0.671$			$\gamma_{UT}=63.657$			$\gamma_{TB}'=0.655$		
	S-L0	$\gamma_{TB}=$*0.251*			$\gamma_{UT}=$*45.029*			$\gamma_{TB}'=0.822$		

The λ_1, λ_2, Λ_1 and Λ_2, are dimensionless ratios. Compared to pure InP, the lower γ_{U1}, γ_{ISF}, γ_{U2}, γ_{ESF}, γ_{U3}, γ_{tTSF}, γ_{TB}, γ_{UT}, λ_1, Λ_1 and larger λ_2, Λ_2 are in italics for S-doped InP

This means that the reduction effects of S dopants on the stable SF energies is local, i.e., only works when S atom dopes in the SF/TB. It is evident that the γ_{TB} could be decreased by ~62.6% when the separate TB doped by S atom. Similarly, the reduction of unstable SF energies also depends strongly on the location of S doping, that is, γ_{U1}(S-L0), γ_{U2}(S-L1), γ_{U3}(S-L2) and γ_{UT}(S-L0). The localized effects of S dopants on the SF energies could be helpful to understand the formation of microtwin in S-doped InP [18].

3.2 The Twinning Ability

Based on the analysis by Tadmor and Hai [19], the twinning tendency could be appraised by the dimensionless ratios $\lambda_1=\gamma_{ISF}/\gamma_{U1}$, and $\lambda_2=\gamma_{U1}/\gamma_{U2}$. The smaller λ_1 and the larger λ_2, the more likely it is to generate a new SF on L1 plane next to the existing ISF (L0 plane) to form ESF. As seen in Table 1, the smaller λ_1 and larger λ_2 for the case of S-L1 compared with pure InP means that the twinning ability of InP is greatly enhanced by S doping due to the simultaneous decreases in γ_{ISF} and γ_{U2}. However, the values of λ_1 and λ_2 for S-L0, S-L2, and S-L3 are comparable with that of pure InP. Apparently, the enhanced ability of twinning, strongly dependent on the location of S atom, is associated with the localized reduction effects of S dopants on the SF energies. Furthermore, the smaller $\Lambda_1=\gamma_{ESF}/\gamma_{U2}$ and larger $\Lambda_2=\gamma_{U2}/\gamma_{U3}$ could make the twinning from ESF to tTSF more possible, which is reasonable based on the derivation by Tadmor and Hai [19] and the weak interaction between neighboring SFs. Compared with pure InP, the enhanced twinning with smaller Λ_1 and larger Λ_2 only present when S atom is doped in L2 layer in order to decrease γ_{ESF}, γ_{U3} simultaneously. At the same time, the twinning ability on the S-L1 plane weakens to be comparable with the pure InP. This suggests that the thickening of microtwin could be facilitated by the gathering of S dopants in SFs/TBs.

3.3 The Segregation of Sulfur Dopants

It is conspicuous that the doping locations of S atom is crucial for the thickening of microtwin in InP. We investigated the capabilities of S dopants segregating to the regions around SF/TB by comparing the energies of supercells with S atom near SF and in the perfect region. Here, more than thirteen-diatomic thick supercells without vacuum were established, and S-L7, far from the SF/TB, was selected as perfect region. Figure 3 shows the preferential locations of S atom segregating are L1 layer for ISF, L2 layer for ESF, consistent with the locations of enhanced ability of twinning by S doping, which confirms that it is possible to thicken microtwin by the segregation of S atom in SFs/TBs. As expected, for tTSF and separate TB, the minimum segregation energy is located in L3 layer and L0 layer, respectively. Meanwhile, the L0 layer, as another TB, is also the easy segregation location for the microtwins though the fluctuation (like in L3 layer) near ISF is present.

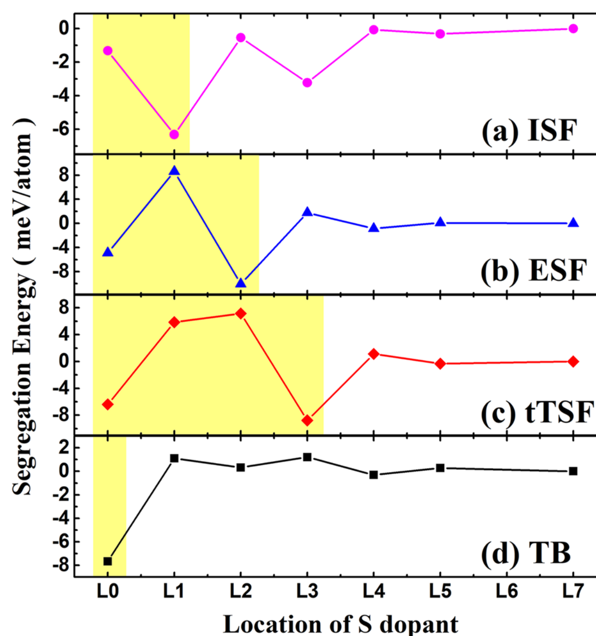

Fig. 3 The segregation energies of S dopant in InP respectively around **a** ISF, **b** ESF, **c** tTSF and **d** separate TB. The SF/TB regions are highlighted by the yellow shadow

The shifting of energy level may be responsible for the segregation tendency. A shallow impurity level will be introduced near the bottom of conduction band when S doping in InP [33]. The segregation of S atom to SF will make this impurity level to move deeper into the bandgap [34]. Consequently, the total energy declines. Another possibility is electric field effect around the TB [35], which could arise from the staggering alignments of energy bands [9, 10]. The ionized S atom could be impelled by the electric field to TB in order to reduce electric energy. Conversely, the electric field may lead to the difficulty of S doping in the thin microtwins, as seen the positive segregation energies on L1 layer for ESF, and on L1, L2 layer for tTSF. Even though, further studies are needed to understand the interaction between dopants and SFs/TBs.

3.4 The Charge Density Analyses

The reduction effects of S dopants on the GSF energy of InP could be attributed to the electronic characteristics of dopants. The well-defined high charge density areas in Fig. 4a suggest that valence electrons are localized strongly to the four covalent bonds in the tetrahedron composed of P and In atoms, of which three bonds across the glide planes. During the production of SFs, the electronic redistribution

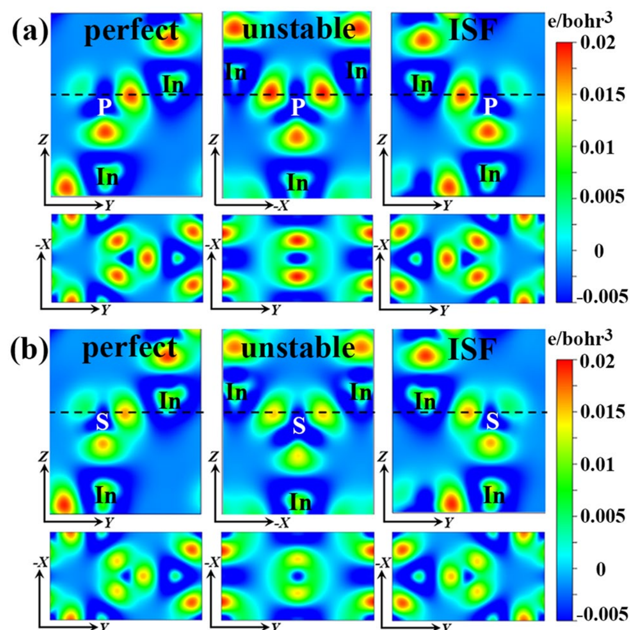

Fig. 4 The charge density difference for perfect, unstable SF, and ISF configurations. **a**, **b** are the situations of pure InP and S-doped InP, respectively. The bottom rows in each panel are the top views of glide planes indicated by the dashed lines in upper cross-section views

mainly occurs in the glide planes, and the charge density on the surrounding planes changes little, which may lead to the weak interaction between neighboring SFs. When the relative shifting of blocks along 1/6<11 $\bar{2}$> initiates, one covalent bond will be stretched, and the other two covalent bonds will be stronger. This may be the main origin of the restoring force during deformation and give rise to the increases of GSF energy. As seen in the top views of Fig. 4a, the areas of high charge density are three in perfect configuration and two in unstable configuration, indicating the stretched bond almost breaks completely in unstable configuration. The electrons mainly flow to the other two bonds to strengthen the interplanar connecting, which is implied by the slightly higher charge density of the two bonds across the glide planes than that of the remaining one bond, as seen in the cross-section view of unstable configuration in Fig. 4a. Therefore, the SF energy reaches the maximum at the unstable SF configuration. When the shifting stabilizes again, reaching ISF configuration, the charge resumes original pattern though the symmetry is different due to the presence of SF.

Naturally, as n-type dopant, S atom has more valence electrons than the replaced P atom. However, comparing the Fig. 4a, b, the charge density of In-S bonds is obviously lower than that of In-P bonds, whether for perfect/stable or unstable configuration. S-doping changes little the charge density of In-P bonds near S-doped plane. Consequently, the interplanar interaction between glide planes is weakened by the S atom, namely the GSF energy of InP is locally decreased by S-doping. The reduced charge density of In-S bonds may be attributed to the weaker localization of electrons in shallow S-dopant level than that in host valence bands because the shallow level is closer to conduction bands. That is to say, the electrons along In-S bonds is easier to transit to conduction bands so as to improve the electronical conductivity of InP crystal, than the electrons along In-P bonds. This reduction effects of S dopants on the GSF energy of InP are consistent with the experimental observation in n-type silicon [31].

4 Conclusion

In summary, we have calculated the GSF energies of pure and S-doped InP. For pure InP, the relationships of $\gamma_{ISF} \approx \gamma_{ESF} \approx \gamma_{tTSF} \approx 2\gamma_{TB}$ and $\gamma_{U1} \approx \gamma_{U2}$ $(\gamma_{U3}) - \gamma_{ISF} \approx \gamma_{UT}$ have been established, which indicates the interaction between neighboring SFs is weak and ESF could be considered as twin embryos based on the convergence of GSF energy curves. In S-doped InP, the charge density of In-S bonds is lower than that of In-P bonds, and thus the GSF energy on S-doped glide plane is decreased considerably, which enhances the twinning ability locally. Furthermore, preferential segregation of S dopants on SF/TB could facilitate the thickening of microtwin. Because of the inevitable encounter with SFs/microtwins in the optoelectronic applications of InP, this work is helpful to understand the effects of n-type dopants on the GSF energy of InP and other III–V compounds.

Acknowledgements This work was supported by the New-round Discipline Construction of SJTU (2018–2020) Grants: "D & R system for Si-based optoelectronic materials and devices"

Compliance with Ethical Standards

Conflict of interest The authors declare they have no conflict of interest.

Availability of Data The data that supports the findings of this study are available within the article.

Code Availability All the calculations were implemented with the Vienna ab-initio simulation package (VASP).

References

1. del Alamo, J.A.: Nanometre-scale electronics with III-V compound semiconductors. Nature. **479**(7373), 317–323 (2011). https://doi.org/10.1038/nature10677
2. Chen, S., Li, W., Wu, J., Jiang, Q., Tang, M., Shutts, S., Elliott, S.N., Sobiesierski, A., Seeds, A.J., Ross, I., Smowton, P.M., Liu, H.: Electrically pumped continuous-wave III–V quantum dot

lasers on silicon. Nat. Photonics. **10**(5), 307–311 (2016). https://doi.org/10.1038/nphoton.2016.21
3. Coldren, L.A., Nicholes, S.C., Johansson, L., Ristic, S., Guzzon, R.S., Norberg, E.J., Krishnamachari, U.: High performance InP-based photonic ICs—a tutorial. J. Lightwave Technol. **29**(4), 554–570 (2011). https://doi.org/10.1109/JLT.2010.2100807
4. Yamamoto, A., Yamaguchi, M., Uemura, C.: High conversion efficiency and high radiation resistance InP homojunction solar cells. Appl. Phys. Lett. **44**(6), 611–613 (1984). https://doi.org/10.1063/1.94851
5. Yamaguchi, M., Uemura, C., Yamamoto, A.: Radiation damage in InP single crystals and solar cells. J. Appl. Phys. **55**(6), 1429–1436 (1984). https://doi.org/10.1063/1.333396
6. Kim, D.S., Forrest, S.R., Lange, M.J., Cohen, M.J., Olsen, G.H., Menna, R.J., Paff, R.J.: Study of InxGa1 – xAs/InAsyP1 – y structures lattice mismatched to InP substrates. J. Appl. Phys. **80**(11), 6229–6234 (1996). https://doi.org/10.1063/1.363699
7. Sun, Y.-T., Kataria, H., Metaferia, W., Lourdudoss, S.: Realization of an atomically abrupt InP/Si heterojunction via corrugated epitaxial lateral overgrowth. CrystEngComm. **16**(34), 7889 (2014). https://doi.org/10.1039/c4ce00844h
8. Wang, F., Wang, C., Wang, Y., Zhang, M., Han, Z., Yip, S., Shen, L., Han, N., Pun, E.Y.B., Ho, J.C.: Diameter dependence of planar defects in InP nanowires. Sci. Rep. **6**(1), 32910 (2016). https://doi.org/10.1038/srep32910
9. Belabbes, A., Panse, C., Furthmüller, J., Bechstedt, F.: Electronic bands of III–V semiconductor polytypes and their alignment. Phys. Rev. B. **86**(7), 075208 (2012). https://doi.org/10.1103/PhysRevB.86.075208
10. Vainorius, N., Jacobsson, D., Lehmann, S., Gustafsson, A., Dick, K.A., Samuelson, L., Pistol, M.-E.: Observation of type-II recombination in single wurtzite/zinc-blende GaAs heterojunction nanowires. Phys. Rev. B. **89**(16), 165423 (2014). https://doi.org/10.1103/PhysRevB.89.165423
11. Wallentin, J., Ek, M., Wallenberg, L.R., Samuelson, L., Borgström, M.T.: Electron trapping in InP nanowire FETs with stacking faults. Nano Lett. **12**(1), 151–155 (2012). https://doi.org/10.1021/nl203213d
12. Pemasiri, K., Montazeri, M., Gass, R., Smith, L.M., Jackson, H.E., Yarrison-Rice, J., Paiman, S., Gao, Q., Tan, H.H., Jagadish, C., Zhang, X., Zou, J.: Carrier dynamics and quantum confinement in type II ZB-WZ InP nanowire homostructures. Nano Lett. **9**(2), 648–654 (2009). https://doi.org/10.1021/nl802997p
13. Qian, X., Kawai, M., Goto, H., Li, J.: Effect of twin boundaries and structural polytypes on electron transport in GaAs. Comput. Mater. Sci. **108**, 258–263 (2015). https://doi.org/10.1016/j.commatsci.2015.06.011
14. Ikonic, Z., Srivastava, G.P., Inkson, J.C.: Optical properties of twinning superlattices in diamond-type and zinc-blende-type semiconductors. Phys. Rev. B. **52**(19), 14078–14085 (1995). https://doi.org/10.1103/PhysRevB.52.14078
15. Gottschalk, H., Patzer, G., Alexander, H.: Stacking fault energy and ionicity of cubic III–V compounds. Phys. Status Solidi A. **45**(1), 207–217 (1978). https://doi.org/10.1002/pssa.2210450125
16. Woodbridge, K.: Heterostructures on Silicon: One Step Further with Silicon, vol. 160. NATO ASI Series. Springer, Dordrecht (1989)
17. Algra, R.E., Verheijen, M.A., Borgstrom, M.T., Feiner, L.F., Immink, G., van Enckevort, W.J., Vlieg, E., Bakkers, E.P.: Twinning superlattices in indium phosphide nanowires. Nature. **456**(7220), 369–372 (2008). https://doi.org/10.1038/nature07570
18. Azzaz, M., Michel, J.-P., George, A.: Plastic deformation, extended stacking faults and deformation twinning in single crystalline indium phosphide 2. S doped InP. Philos. Mag. A. **73**(3), 601–624 (1996). https://doi.org/10.1080/01418619608242986
19. Tadmor, E.B., Hai, S.: A Peierls criterion for the onset of deformation twinning at a crack tip. J. Mech. Phys. Solids. **51**(5), 765–793 (2003). https://doi.org/10.1016/s0022-5096(03)00005-x
20. De Cooman, B.C., Estrin, Y., Kim, S.K.: Twinning-induced plasticity (TWIP) steels. Acta Mater. **142**, 283–362 (2018). https://doi.org/10.1016/j.actamat.2017.06.046
21. Glas, F.: A simple calculation of energy changes upon stacking fault formation or local crystalline phase transition in semiconductors. J. Appl. Phys. **104**(9), 093520 (2008). https://doi.org/10.1063/1.3009338
22. Vítek, V.: Intrinsic stacking faults in body-centred cubic crystals. Philos. Mag. **18**(154), 773–786 (1968). https://doi.org/10.1080/14786436808227500
23. Tian, L.-Y., Lizárraga, R., Larsson, H., Holmström, E., Vitos, L.: A first principles study of the stacking fault energies for fcc Co-based binary alloys. Acta Mater. **136**, 215–223 (2017). https://doi.org/10.1016/j.actamat.2017.07.010
24. Kresse, G., Furthmüler, J.: Efficient iterative schemes for ab initio total-energy calculations using a plane-wave basis set. Phys. Rev. B. **54**(16), 11169–11186 (1996). https://doi.org/10.1103/PhysRevB.54.11169
25. Blöchl, P.E.: Projector augmented-wave method. Phys. Rev. B. **50**(24), 17953–17979 (1994). https://doi.org/10.1103/physrevb.50.17953
26. Perdew, J.P., Burke, K., Ernzerhof, M.: Generalized gradient approximation made simple. Phys. Rev. Lett. **77**(18), 3865–3868 (1996). https://doi.org/10.1103/PhysRevLett.77.3865
27. Massidda, S., Continenza, A., Freeman, A.J., de Pascale, T.M., Meloni, F., Serra, M.: Structural and electronic properties of narrow-band-gap semiconductors: InP, InAs, and InSb. Phys. Rev. B. **41**(17), 12079–12085 (1990). https://doi.org/10.1103/PhysRevB.41.12079
28. Branicio, P.S., Rino, J.P., Gan, C.K., Tsuzuki, H.: Interaction potential for indium phosphide: a molecular dynamics and first-principles study of the elastic constants, generalized stacking fault and surface energies. J. Phys. Condens. Matter. **21**(9), 095002 (2009). https://doi.org/10.1088/0953-8984/21/9/095002
29. Ogata, S., Li, J., Yip, S.: Energy landscape of deformation twinning in bcc and fcc metals. Phys. Rev. B. **71**(22), 224102 (2005). https://doi.org/10.1103/PhysRevB.71.224102
30. Kibey, S., Liu, J.B., Johnson, D.D., Sehitoglu, H.: Generalized planar fault energies and twinning in Cu–Al alloys. Appl. Phys. Lett. **89**(19), 191911 (2006). https://doi.org/10.1063/1.2387133
31. Ohno, Y., Taishi, T., Tokumoto, Y., Yonenaga, I.: Interaction of dopant atoms with stacking faults in silicon crystals. J. Appl. Phys. **108**(7), 073514 (2010). https://doi.org/10.1063/1.3490753
32. Sato, M., Sumino, K., Hiraga, K.: Impurity effect in stacking fault energy of silicon crystals studied by high resolution electron microscopy. Phys. Status Solidi A. **68**(2), 567–577 (1981). https://doi.org/10.1002/pssa.2210680228
33. Yoshinaga, H., Matsumori, T., Uehara, F.: Impurity Effect on Recombination Processes in InP. Jpn. J. Appl. Phys. **35**(Part 1, No. 5B), 2930–2933: (1996). https://doi.org/10.1143/jjap.35.2930
34. Yamamoto, Y., Togase, K., Ohno, Y., Yonenaga, I., Nishitani, S.R.: First principles calculations of solution energies of dopants around stacking faults in Si crystal. Jpn. J. Appl. Phys. **53**(6), 061302 (2014). https://doi.org/10.7567/jjap.53.061302
35. Bao, J., Bell, D.C., Capasso, F., Wagner, J.B., Mårtensson, T., Trägårdh, J., Samuelson, L.: Optical properties of rotationally twinned InP nanowire heterostructures. Nano Lett. **8**(3), 836–841 (2008). https://doi.org/10.1021/nl072921e

Publisher's Note Springer Nature remains neutral with regard to jurisdictional claims in published maps and institutional affiliations.